Charge-Transfer Complexes

$[\{[Pt(en)_2][PtX_2(en)_2]\}_3][\{(MX_5)X_3\}_2]\cdot 12H_2O$: Quasi-One-Dimensional Halogen-Bridged Pt^{II}–Pt^{IV} Mixed-Valence Compounds with Magnetic Counteranions**

Masahiro Yamashita, Daisuke Kawakami, Satoshi Matsunaga, Yoshio Nakayama, Mari Sasaki, Shinya Takaishi, Fumiyasu Iwahori, Hitoshi Miyasaka, Ken-ichi Sugiura, Yoshiki Wada, Hiroshi Miyamae, Hiroyuki Matsuzaki, Hiroshi Okamoto, Hisaaki Tanaka, Kazuhiro Marumoto, and Shin-ichi Kuroda*

Quasi-one-dimensional, halogen-bridged mixed-valence compounds (MX chains) have recently attracted much

[*] Prof. M. Yamashita, D. Kawakami, S. Matsunaga, Y. Nakayama, M. Sasaki, Dr. S. Takaishi, Dr. F. Iwahori, Dr. H. Miyasaka, Prof. K.-i. Sugiura
Department of Chemistry
Graduate School of Science
Tokyo Metropolitan University and CREST(JST)
1-1 Minamiosawa, Hachioji, Tokyo 192-0397 (Japan)
Fax: (+81) 426-77-2525
E-mail: yamashit@comp.metro-u.ac.jp

Dr. Y. Wada
Advanced Materials Laboratory
National Institute for Materials Science
1-1 Namiki, Tsukuba, Ibaraki 305-0044 (Japan)

Prof. H. Miyamae
Faculty of Science
Josai University
1-1 Keyakidai, Sakado, Saitama 350-0295 (Japan)

Dr. H. Matsuzaki, Prof. H. Okamoto
Department of Advanced Materials Science
Graduate School of Frontier Science
The University of Tokyo
Kashiwa, Chiba 277-8561 (Japan)

Dr. H. Tanaka, Dr. K. Marumoto, Prof. S. Kuroda
Department of Applied Physics
Graduate School of Engineering
Nagoya University
Furocho, Chikusa-ku, Nagoya, Aichi 464-8603 (Japan)

[**] This work was partly supported by a Grant-in Aid for Creative Scientific Research from the Ministry of Education, Culture, Sports, Science, and Technology. We are grateful to Dr. Noboru Kishi of the Rigaku Corporation for measuring the temperature dependence of the X-ray powder-diffraction patterns. en = ethylenediamine; M = Co^{2+}, Mn^{2+}, and Fe^{2+}; X = Cl^- and Br^-.

 DOI: 10.1002/ange.200460580

attention because they show very interesting physical properties, such as intense and dichroic intervalence charge-transfer bands, overtone progression of resonance-Raman spectra, luminescence spectra with large Stokes shifts, large third-order nonlinear optical properties, mid-gap absorptions attributable to solitons and polarons, etc., and because they are one-dimensional model compounds of high-critical-temperature (T_c) copper oxide superconductors.[1–9] Theoretically, these MX chains are considered as Peierls–Hubbard systems where the electron–phonon interaction (S), the electron transfer (T), and the intra- and intersite Coulomb repulsion energies (U and V, respectively) compete or cooperate with each other.[10,11] Platinum and palladium compounds form charge-density-wave (CDW) states or M^{II}–M^{IV} mixed-valence states as a result of electron–phonon interactions (S), where the bridging halogen atoms are displaced from the midpoint between the two neighboring metal ions. Accordingly, the half-filled metallic band splits into an occupied valence band and an unoccupied conduction band with finite Peierls energy gaps. Therefore, these compounds belong to class II in the Robin–Day classification of mixed-valence complexes.[1] In these MX chain compounds the CDW amplitudes can be tuned by varying the metal ions, bridging halogen atoms, in-plane ligands, and counteranions.[12] Although more than 200 mixed-valence platinum compounds have been synthesized so far, all these MX chain compounds have closed-shell or nonmagnetic counteranions such as ClO_4^-, BF_4^-, or halogen ions. In this study we have succeeded in synthesizing the novel Pt^{II}–Pt^{IV} mixed-valence complexes $[\{[Pt(en)_2][PtX_2(en)_2]\}_3][\{(MX_5)X_3\}_2]\cdot 12\,H_2O$ ($M = Co^{2+}$, Mn^{2+}, and Fe^{2+}; $X = Cl^-$ and Br^-; en = ethylenediamine) with magnetic counteranions. At the same time, a unique packing motif as well as an interesting adsorption–desorption of water molecules has been observed. Herein, we describe the syntheses, crystal structures, thermogravimetric analysis (TGA), temperature dependence of X-ray powder-diffraction patterns, single-crystal reflectance spectra, resonance-Raman spectra, and electron spin resonance (ESR) spectra of these complexes.

Single-crystal X-ray structural determinations were carried out for $[\{[Pt(en)_2][PtCl_2(en)_2]\}_3][\{(MnCl_5)Cl_3\}_2]\cdot 12\,H_2O$. Figure 1 shows two perspective views of this complex. The planar $\{Pt(en)_2\}$ units are bridged by halogen ions which are disordered at positions away from the midpoints between two neighboring Pt ions with half occupancies, thus forming linear chain Pt^{II}–Pt^{IV} mixed-valence structures (one of the distorted Cl ions has been omitted for clarity). The Pt···Pt distance and Pt^{IV}–Cl and Pt^{II}···Cl bond lengths are 5.303 Å, 2.325 Å, and 2.978 Å, respectively, while those in $[\{Pt(en)_2\}\{PtCl_2(en)_2\}](ClO_4)_4$ are 5.403 Å, 2.318 Å, and 3.085 Å, respectively.[13] Therefore, the degrees of distortions of the bridging halogen atoms from the midpoints between two neighboring Pt ions, defined as $d(Pt^{IV}–Cl)/d(Pt^{II}\cdots Cl)$, are 0.78 for the former compound and 0.75 for the latter, thus indicating that the oxidation state of the magnetic counteranion complex is closer to Pt^{III}, namely a Robin–Day class III complex, than the ClO_4^- compound.[1] The magnetic $MnCl_5$ counterions have a trigonal-bipyramidal structure. The Mn–Cl bond lengths range from 2.457 Å in the plane to 2.495 Å along the axis. The Cl_3 ions form a triangular structure, with a Cl···Cl distance in this triangle of 6.051 Å. These MCl_5 and Cl_3 ions stack alternately along the main Pt^{II}–Pt^{IV} chains. Hydrogen bonds between the H atoms of the en ligands and the

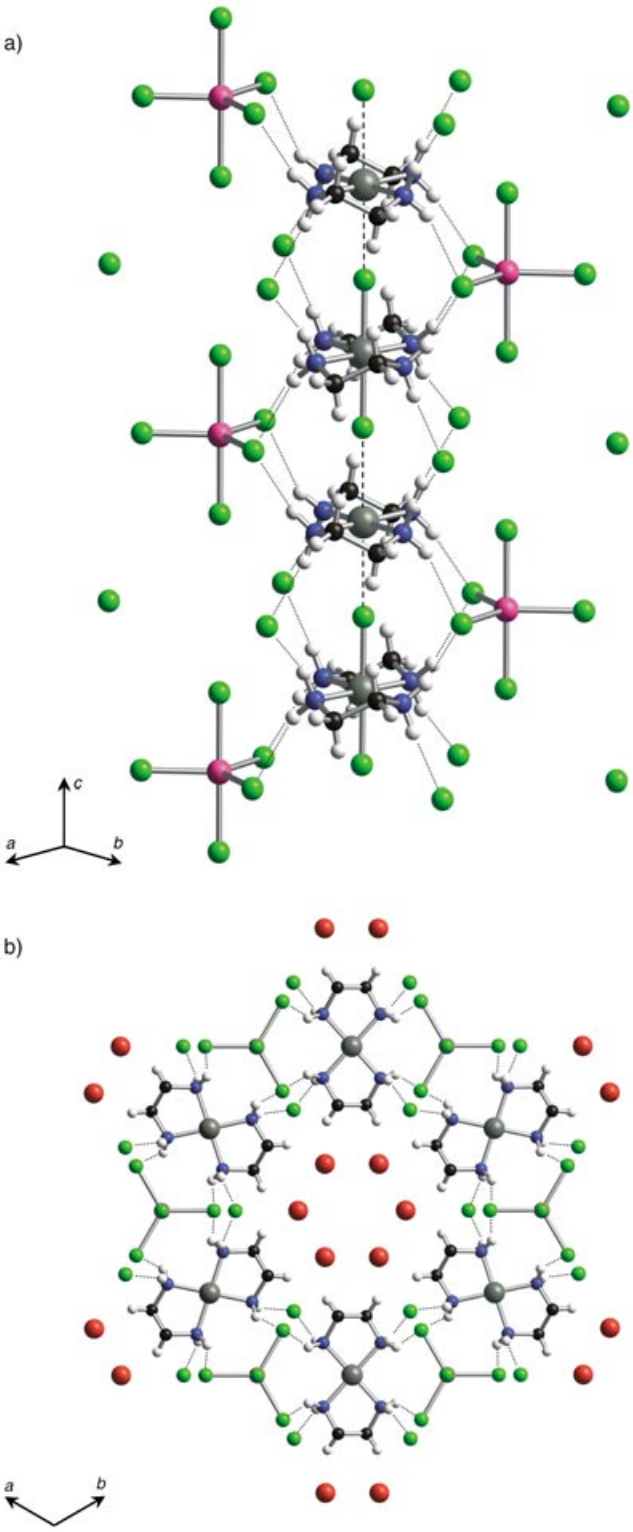

Figure 1. Perspective views of the 3D packing of $[\{[Pt(en)_2][PtCl_2(en)_2]\}_3][\{(MnCl_5)Cl_3\}_2]\cdot 12\,H_2O$; H white, C black, N blue, O red, Mn pink, Cl green, Pt gray. One of the disordered Cl ions has been omitted for clarity. Dotted and broken lines represent hydrogen bonds and Pt^{II}···Cl interactions, respectively.

Cl atoms of $MnCl_5$ are observed (H···Cl = 2.526 Å), as are hydrogen bonds between these H atoms and the Cl atoms of the Cl_3 unit (H···Cl = 2.471 Å). As shown in Figure 1b, the Pt chains and counteranions form hexagonal spaces, which are filled with water molecules. Although only six water molecules are observed in the crystal structure, the presence of 12 water molecules per molecular unit was confirmed by thermogravimetric analysis (TGA) and elemental analysis (see below). All 12 water molecules were observed in the solid-state structure of $[\{[Pt(en)_2][PtBr_2(en)_2]\}_3][\{(MnBr_5)Br_3\}_2]\cdot 12H_2O$. A preliminary structure determination of the other compounds was also carried out. Although they have not been completely solved, their essential structures are the same as that of $[\{[Pt(en)_2][PtCl_2(en)_2]\}_3][\{(MnCl_5)Cl_3\}_2]\cdot 12H_2O$.

To clarify the desorption behavior of the water molecules a TGA study was performed on $[\{[Pt(en)_2][PtCl_2(en)_2]\}_3][\{(MnCl_5)Cl_3\}_2]\cdot 12H_2O$ (Figure 2). Upon heating the sample

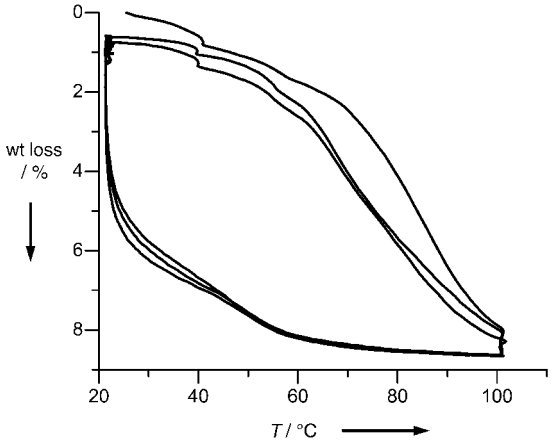

Figure 2. TGA plots of $[\{[Pt(en)_2][PtCl_2(en)_2]\}_3][\{(MnCl_5)Cl_3\}_2]\cdot 12H_2O$.

from 20 to 100 °C, at a rate of 3 °C min^{-1}, the sample weight gradually decreased. This weight loss of approximately 8% can be attributed to the loss of water molecules, and is in good agreement with the desorption of 12 water molecules per molecular unit (7.2%). After keeping the temperature at 100 °C for 60 min, the sample was cooled down to 20 °C at a rate of 3 °C min^{-1}. The weight of the sample gradually increased and became almost the same as that of the initial sample. This result indicates that the 12 desorbed water molecules can re-enter the crystals reversibly. We confirmed this reversibility by repeating the process three times. The weight loss during the first heating stage is a little larger than those during the second and third stages. This can be accounted for by desorption of impurities from the crystal surface.

Temperature-dependent X-ray powder-diffraction patterns were measured in order to confirm that the crystal structure is maintained even in the absence of water molecules. Figure 3 shows X-ray powder-diffraction patterns of $[\{[Pt(en)_2][PtCl_2(en)_2]\}_3][\{(MnCl_5)Cl_3\}_2]\cdot 12H_2O$ at various temperatures. The peaks of these patterns remain sharp and their positions do not change during the heating and cooling

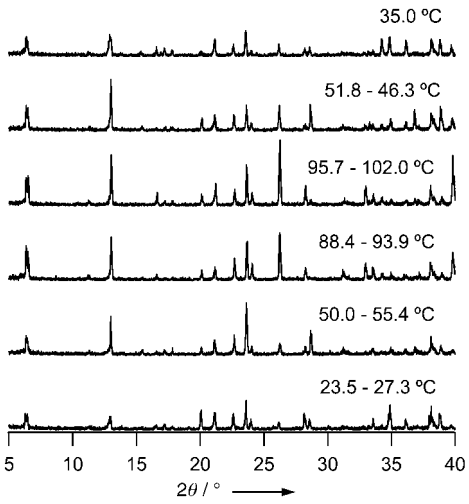

Figure 3. Temperature dependence of the X-ray powder-diffraction patterns in $[\{[Pt(en)_2][PtCl_2(en)_2]\}_3][\{(MnCl_5)Cl_3\}_2]\cdot 12H_2O$.

processes, thus indicating that the crystal structure is sustained even in the absence of water molecules.

The single-crystal reflectance spectra of $[\{[Pt(en)_2][PtCl_2(en)_2]\}_3][\{(MnCl_5)Cl_3\}_2]\cdot 12H_2O$ and $[\{[Pt(en)_2][PtBr_2(en)_2]\}_3][\{(MBr_5)Br_3\}_2]\cdot 12H_2O$ (M = Mn and Co) were measured at room temperature. Their optical conductivities obtained from the Kramers–Kronig transformation are shown in Figure 4. The Cl- and Br-bridged compounds show

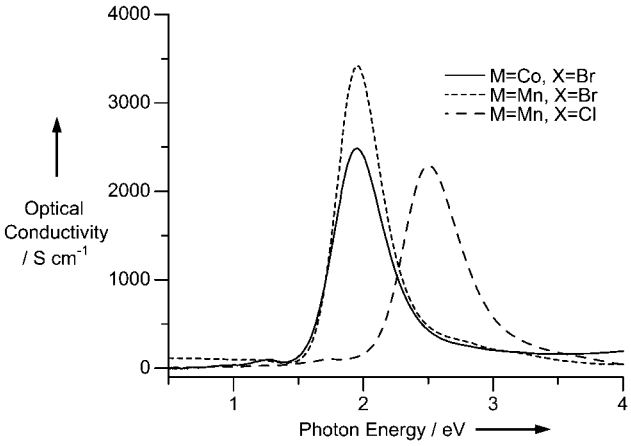

Figure 4. Optical conductivity spectra of $[\{[Pt(en)_2][PtCl_2(en)_2]\}_3][\{(MnCl_5)Cl_3\}_2]\cdot 12H_2O$ and $[\{[Pt(en)_2][PtCl_2(en)_2]\}_3][\{(MnBr_5)Br_3\}_2]\cdot 12H_2O$ (M = Mn and Co).

dichroic, intense bands at 2.50 eV and 1.95 eV, respectively. These are attributable to the charge-transfer (CT) transition from the Pt^{II} species to the Pt^{IV} species along the chain. According to theoretical studies,[14,15] the energy position of the CT bands in mixed-valence compounds can be given by $2S-U$ if T and V are neglected. The lower CT energy of the Mn compound than the ClO_4 compound (2.72 eV) could be a consequence of a decrease of S, thus indicating that the charge delocalization of this compound is greater than that of the

ClO_4 compound; this proposal is consistent with the X-ray crystal structures. The CT energies of the Br-bridged compounds are lower than those of the Cl-bridged compounds because of their greater charge delocalization.

Overtone progressions attributable to the Pt^{IV}–X stretching modes are observed in the resonance-Raman spectra, where the stretching modes of the Cl- and Br-bridged compounds occur at about 310 cm^{-1} (310.1 cm^{-1} for Mn and Fe) and 175 cm^{-1} (177.1 cm^{-1} for Mn, 175.7 cm^{-1} for Fe, and 175.7 cm^{-1} for Co), respectively. The lower value of the stretching mode of $[\{[Pt(en)_2][PtCl_2(en)_2]\}_3][\{(MnCl_5)Cl_3\}_2]\cdot 12H_2O$ than that of the ClO_4 compound (311.3 cm^{-1}) could be the result of an increase in the anharmonicity of the potential energy surface, thus indicating that electronic delocalization of the Mn compound is greater than that of the ClO_4 compound, as predicted in a previous theoretical study.[15] This fact is consistent with the crystal structure and the optical-conductivity results.

Temperature-dependent (M = Co, X = Br) and angle-dependent (M = Mn, X = Cl) ESR spectra are shown in Figure 5. Polycrystalline samples of the Co salt were used. The ESR spectra depend highly on the metal species, and their intensity decreases with increasing temperature following the Curie law. The nearly symmetrical line-shape for the Co salt with a mean g value of about 4.9 indicates that the g factor is nearly isotropic—the magnetic-field difference arising from the anisotropic g values for polycrystalline samples is less than the linewidth. In general, the free Co^{2+} ion has a ^4F state ($S = {}^3/_2$) and the orbital triplet becomes the lowest state in the cubic crystal-field symmetry. However, these degenerate levels are split both by a lower symmetry of the crystal field, such as tetragonal or trigonal, and spin–orbit coupling. As a result, six Kramer's doublets ($S = {}^1/_2$) are created and each level can be represented by a "fictitious spin ${}^1/_2$".[16,17] In this case, the inter-level mixing with the excited states lying close to the ground-state Kramer's doublet causes the large g shift from the free-electron g value (2.0023); the broadening of the spectrum as the temperature is raised is a consequence of the shortening of the spin–lattice relaxation time (Figure 5a). In the case of the Mn salt the ESR spectrum is spread over a wide magnetic-field range with several splittings; the spectral shape is almost unchanged within the measured temperature range. Such a situation may be caused by the zero-field splitting of the high-spin Mn^{2+} ion ($S = {}^5/_2$). We also note that the total span of the signal splitting is a maximum at 0 and 180° from the chain axis, thus indicating that the axis of the dipolar interaction coincides with the chain direction. The ESR signals for the Co and Mn salts are ascribed to the M sites, which confirms the successful synthesis of the 1D electronic system with magnetic counteranions.

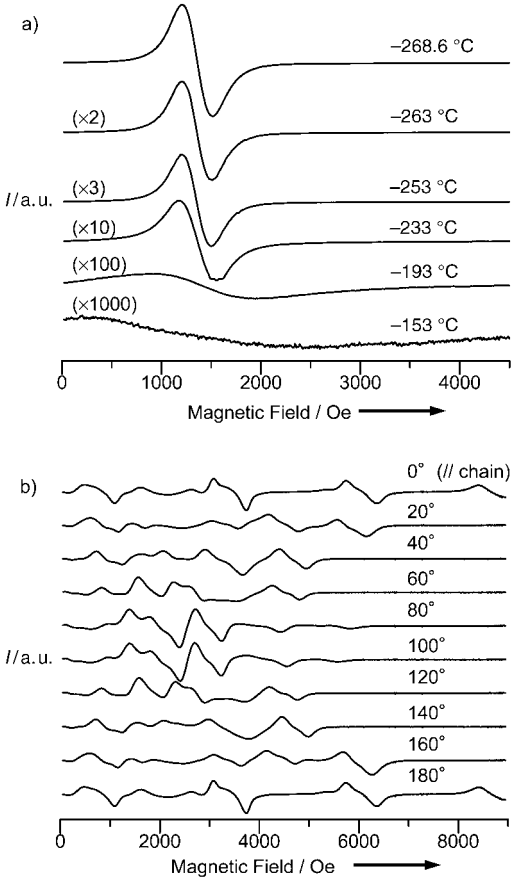

Figure 5. Temperature- and angle-dependence of the ESR spectra of $[\{[Pt(en)_2][PtX_2(en)_2]\}_3][\{(MX_5)X_3\}_2]\cdot 12H_2O$: a) M = Co^{2+}, X = Br; b) M = Mn^{2+}, X = Cl.

In summary, we have succeeded in synthesizing mixed-valence Pt^{II}–Pt^{IV} compounds with magnetic counteranions. These magnetic MX_5 counterions (M = Mn^{2+}, Fe^{2+}, Co^{2+}; X = Cl^-, Br^-) have an unusual trigonal-bipyramidal structure. The complexes have hexagonal micropores, similar to zeolites, which contain 12 water molecules per molecular unit. These water molecules can be desorbed by heating the complexes to 100 °C whilst maintaining the skeletal structure; they can be adsorbed again by cooling to 20 °C. The ESR spectra reflect the variety of the spin species in the counteranions.

Experimental Section

The compounds were synthesized by adding 150 mg (0.76 mmol) of MX_2 and 1.5 ml HX to an aqueous solution (1 ml) containing 100 mg (0.26 mmol) $[Pt(en)_2]X_2$ and 120 mg (0.26 mmol) $[PtX_2(en)_2]X_2$. Lustrous, needle-shaped crystals were obtained after a week. The elemental analyses are as follows: calcd for $C_{24}H_{120}Cl_{22}Mn_2N_{24}O_{12}Pt_6$: C 9.62, H 4.03, N 11.21; found: C 9.52, H 3.75, N 11.07; calcd for $C_{24}H_{120}Cl_{22}Fe_2N_{24}O_{12}Pt_6$: C 9.61, H 4.03, N 11.21; found: C 9.41, H 3.69, N 11.08; calcd for $C_{24}H_{120}Br_{22}Mn_2N_{24}O_{12}Pt_6$: C 7.25, H 3.04, N 8.46; found: C 7.11, H 2.94, N 8.23; calcd for $C_{24}H_{120}Br_{22}Fe_2N_{24}O_{12}Pt_6$: C 7.25, H 3.04, N 8.45; found: C 7.08, H 2.79, N 8.17; calcd for $C_{24}H_{120}Br_{22}Co_2N_{24}O_{12}Pt_6$: C 7.24, H 3.04, N 8.44; found: C 7.03, H 2.84, N 8.34.

X-ray crystallographic analyses of $[\{[Pt(en)_2][PtX_2(en)_2]\}_3][\{(MX_5)X_3\}_2]\cdot 12H_2O$ (M = Co^{2+}, Mn^{2+}, and Fe^{2+}; X = Cl^- and Br^-) were performed with a Rigaku RAXIS-RAPID imaging plate diffractometer equipped with graphite monochromated $Mo_{K\alpha}$ radiation ($\lambda = 0.7107$ Å). Crystal data of $[\{[Pt(en)_2][PtX_2(en)_2]\}_3][\{(MnCl_5)Cl_3\}_2]\cdot 6H_2O$: $C_{24}H_{108}Cl_{22}Mn_2N_{24}O_6Pt_6$, $M_r = 2889.60$, hexagonal, $P6_3/mmc$ (no. 194), $T = 156 \pm 1$ K, $a = 16.0035(6)$, $b = 16.0035(6)$, $c = 10.9333(5)$ Å, $\gamma = 120°$, $V = 2424.0(2)$ Å^3, $Z = 1$, $\rho_{calcd} = 2.078$, final $R = 0.030$, $wR = 0.029$, GOF = 0.985 with $I > 3.00\sigma(I)$. CCDC-238001 contains the supplementary crystallographic data for this paper. These data can be obtained free of charge at www.ccdc.cam.ac.uk/conts/retrieving.html [or from the Cambridge

Crystallographic Data Centre, 12 Union Road, Cambridge CB2 1EZ, UK; Fax: (+44) 1223-336-033; E-mail: deposit@ccdc.cam.ac.ukTGA was performed with a Rigaku DSC 8230L calorimeter. X-ray powder diffraction measurements were recorded with a Rigaku RINT UltimaII + DSC equipment. ESR spectra were measured with a Bruker EMX spectrometer equipped with a gas-flow type cryostat Oxford ESR 900.

Received: May 7, 2004

Keywords: bridging ligands · charge transfer · EPR spectroscopy · mixed-valent compounds · zeolite analogues

[1] M. B. Robin, P. Day, *Adv. Inorg. Chem. Radiochem.* **1967**, *10*, 247–297.
[2] H. Tanino, K. Kobayashi, *J. Phys. Soc. Jpn.* **1983**, *52*, 1446–1456.
[3] A. R. Bishop, B. L. Swanson, *Los Alamos Sci.* **1993**, *21*, 133–143.
[4] R. J. H. Clark, *Adv. Infrared Raman Spectrosc.* **1983**, *11*, 95–132.
[5] H. Okamoto, M. Yamashita, *Bull. Chem. Soc. Jpn.* **1998**, *71*, 2023–2039.
[6] M. Yamashita, T. Manabe, T. Kawashima, H. Okamoto, H. Kitagawa, *Coord. Chem. Rev.* **1999**, *190–192*, 309–330.
[7] N. Kuroda, M. Sakai, Y. Nishina, M. Tanaka, S. Kurita, *Phys. Rev. Lett.* **1987**, *58*, 2122–2125.
[8] H. Okamoto, T. Mitani, K. Toriumi, M. Yamashita, *Phys. Rev. Lett.* **1992**, *69*, 2248–2251.
[9] R. J. Donohoe, L. A. Worl, C. A. Arrington, A. Bulou, B. I. Swanson, *Phys. Rev. B: Condens. Matter* **1992**, *45*, 13185–13195.
[10] D. Baeriswyl, A. R. Bishop, *J. Phys. C: Solid State Phys.* **1988**, *21*, 339–356.
[11] A. Mishima, K. Nasu, *Phys. Rev. B: Condens. Matter* **1989**, *39*, 5758–5762.
[12] H. Okamoto, K. Toriumi, K. Okaniwa, T. Mitani, M. Yamashita, *Mater. Sci. Eng.* **1992**, *B13*, L9–L14.
[13] H. Okamoto, M. Yamashita, *Bull. Chem. Soc. Jpn.* **1998**, *71*, 2023–2039.
[14] K. Prassides, P. Shatz, K. Wong, P. Day, *J. Phys. Chem.* **1986**, *90*, 5588–5597.
[15] K. Prassides, P. Shatz, *Chem. Phys. Lett.* **1991**, *178*, 227–234.
[16] A. Abragam, M. H. L. Pryce, *Proc. R. Soc. London* **1951**, *206*, 173–191.
[17] S. Kuroda, M. Motokawa, M. Date, *J. Phys. Soc. Jpn.* **1978**, *44*, 1797–1803.

